Long Term Behavior of Lithographically Prepared *In Vitro* Neuronal Networks

Ronen Segev,[1] Morris Benveniste,[2] Eyal Hulata,[1] Netta Cohen,[3] Alexander Palevski,[1]
Eli Kapon,[1,4] Yoash Shapira,[1] and Eshel Ben-Jacob[1,*]

[1]*School of Physics and Astronomy, Raymond & Beverly Sackler Faculty of Exact Sciences, Tel-Aviv University, Tel-Aviv 69978, Israel*
[2]*Department of Physiology & Pharmacology, Sackler Faculty of Medicine, Tel-Aviv University, Tel-Aviv 69978, Israel*
[3]*Department of Zoology, Wise Faculty of Life Sciences, Tel-Aviv University, Tel-Aviv 69978, Israel*
[4]*Department of Physics, Swiss Federal Institute of Technology Lausanne (EPFL), 1015 Lausanne, Switzerland*

(Received 21 June 2001; published 4 March 2002)

We measured the long term spontaneous electrical activity of neuronal networks with different sizes, grown on lithographically prepared substrates and recorded with multi-electrode-array technology. The time sequences of synchronized bursting events were used to characterize network dynamics. All networks exhibit scale-invariant Lévy distributions and long-range correlations. These observations suggest that different-size networks self-organize to adjust their activities over many time scales. As predictions of current models differ from our observations, this calls for revised models.

DOI: 10.1103/PhysRevLett.88.118102 PACS numbers: 87.17.Nn, 05.70.Ln, 82.40.Bj

The functional organization of (biological) neuronal networks has been the focus of much *in vivo* and *in vitro* research. The ability to process information of neuronal networks derives from their individual abilities to generate temporal sequences of action potentials and to modulate the level and patterns of activity at the network level [1]. *In vivo* cortical studies have revealed physical and functional organizational structures on length scales of $\sim$1 mm [2]. To understand the principles underlying this organizational process, it is important to examine the effect of network size on temporal patterns of activity. *In vitro* neuronal networks provide a relatively simple, self-contained system for examining such questions over a wide range of time scales and network sizes under stable, controlled conditions.

In vitro neural networks exhibit rich spontaneous and stimulated spatiotemporal activity, which are both characterized by synchronized bursting events (SBEs) [3]. During these events, many neurons participate in rapid firing within a brief $\sim$100-ms time window. SBEs are separated by sporadic firing of individual neurons. In many ways, SBEs characterize neuronal network dynamics in analogy to the action potential description of activity at the level of an individual neuron.

To study the connection between network spatial organization and temporal behavior, we have developed a novel lithography method and studied three lithographically prepared networks [4] with different geometries and sizes: (1) *small* 50-cell networks with a quasi-1D 2 mm $\times$ 50 μm geometry, (2) *medium* 10^4-cell networks, with a rectangular 2 mm $\times$ 2 mm geometry, and (3) *large* $2 \cdot 10^6$-cell networks, with a circular 11-mm-radius geometry (Fig. 1). The spontaneous activity of the networks was noninvasively recorded with a 60-electrode multielectrode array (MEA) [5–8]. By growing the dissociated neuronal culture on top of the array, the neurons formed capacitive coupling to the electrodes, enabling the recording of action potentials. Then, the electrode array was placed in a special incubating chamber (our design) for long-term (weeks) recording [4]. Recordings from ten cultures lasting 4–10 days are presented. These recordings summarize

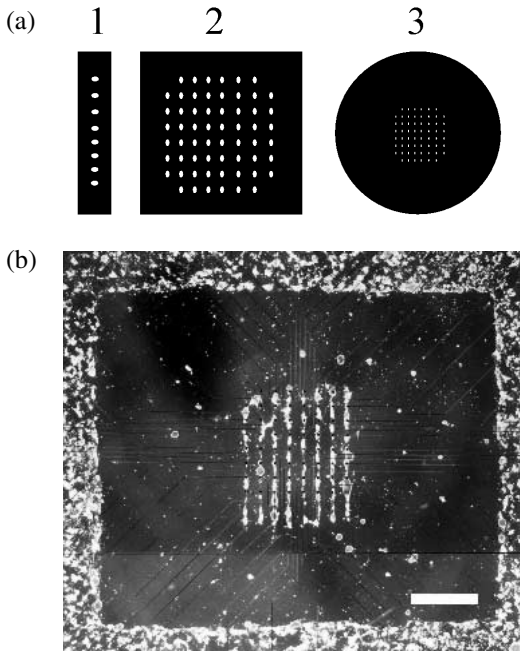

FIG. 1. (a) Schematic description of the three networks geometries and the corresponding electrode layout (relative size is not conserved): (1) a small quasi-1D network, (2) a medium rectangular network, and (3) a large circular network. All electrodes have 30-μm width and are separated by 200 μm. (b) An example of eight quasi-1D networks grown atop a multielectrode array: Each line is a quasi-1D network. Any network with suspected cross talk (e.g., three left columns) were omitted from the analysis. To ensure the survival of the networks, large networks were grown on the periphery of the dish which is disconnected from the quasi-1D networks in the center (scale bar = 1 mm). A similar layout was used for rectangular networks, dissociated from the surrounding network.

the activity of the networks over 8 decades of time (from ms to days).

While neurons' activity can be characterized by interspike intervals (ISI) as we describe below, the network activity needs an appropriate observable to be defined. To do so, the recorded activity can be visualized in raster plots (Fig. 2) which clearly show the appearance of synchronized bursts. For each network, therefore, we first generated the SBE time sequence. In each raster plot, we summed over the number of neural spikes within windows of 100 ms. A time bin in which the spike count exceeds a prespecified threshold is defined as a synchronized bursting event (Fig. 2a, bottom panel). The same sequence can also be presented by the interevent intervals (IEI): $\mathrm{IEI}(n) \equiv t_n - t_{n-1}$ (in analogy to the ISI definition).

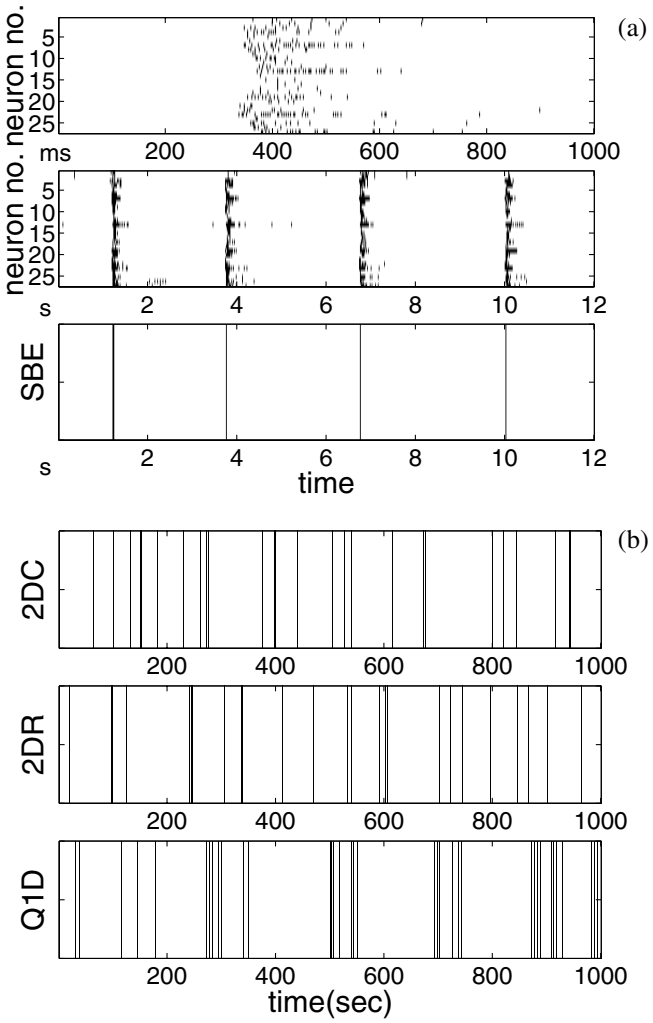

FIG. 2. (a) A raster plot summarizing the activity of 27 neurons during 1 s (top) and 12 s (middle) is shown to illustrate SBE detection. The time axis is divided into bins of 1 ms and 5 ms, respectively. A black line is plotted whenever a neuron fired at least once during the time bin. The top panel is an expansion of the third event (middle). A SBE detected whenever the number of firing neurons in 100-ms time bins exceeds a threshold (usually fixed at 80% of the total number of active neurons). Thus, a time series of SBEs is obtained. (b) Examples of SBE trains from the three network types: large (top, 2D circular), medium (middle, 2D rectangular), and small (bottom, quasi-1D).

SBE mean densities of approximately 1 event/10 s were found in all network sizes and irrespective of the details of the sequence structure. As Fig. 2 shows, however, the smaller the network, the higher the variance of IEI. To examine the temporal patterns of activity in the different networks, analysis was performed on three different time ranges, ISI time scales of 1–100 ms, IEI time scales of 1–100 s, and longer time scales of (up to 10 h). A plot of ISI and IEI distributions indicates that neural and network activities are characterized by a non-Gaussian heavy-tail interval distribution (not shown), indicating possible temporal scaling behavior.

Dynamical systems composed of a large number of nonlinearly coupled subsystems often obey the Lévy distribution [9–11]. Such scaling behavior is also characteristic of some biological systems, at the level of single cells and networks [12,13]. In order to test whether our neuronal networks also fall within this category, fits to the Lévy distribution were performed for single cell as well as for network activity. In either case, the appropriate observable was selected for fitting.

On the neuron level, the activity is represented by the ISI sequence. To study the temporal scaling behavior, the distribution of ISI increments was introduced:

$$\delta(i) = \mathrm{ISI}(i) - \mathrm{ISI}(i-1). \tag{1}$$

Unlike the ISI, δ has a stationary zero mean and is symmetrically distributed. We verified these properties by measuring the stability over a moving window of 10 h. The Lévy distribution $P_{\alpha\gamma}$ of $\delta(i)$ is given by

$$P_{\alpha\gamma}(\delta) = \frac{1}{\pi}\int_0^\infty \exp(-\gamma q^\alpha)\cos(q\delta)\,dq\,, \tag{2}$$

where $0 < \alpha \leq 2$ is the index of stability, which determines the long-tail decay of the distribution, and $\gamma > 0$ is a scale factor, which determines the location of the bending point of the Lévy distribution. Special cases of the Lévy distribution are the Gaussian distribution ($\alpha = 2$) and the Cauchy distribution ($\alpha = 1$). The probability density function (pdf) of $\delta(i)$ for neurons in the small networks is well fitted with the Lévy distribution over 3–4 decades. The behavior of the medium and large size networks is more complex. Their pdfs are well fitted with Lévy distributions for three time decades (Fig. 3a). Above the characteristic SBE width ($\sim$100 ms), the pdf deviates from the fit to the Lévy distribution.

Following the analogy between the action potential and the SBE, the distribution of IEI increments is now considered:

$$\Delta(i) = \mathrm{IEI}(i) - \mathrm{IEI}(i-1). \tag{3}$$

Again, we find that the $\Delta(i)$ pdf of the three network types is well fitted with the Lévy distribution over four time decades, each with its own distribution parameters

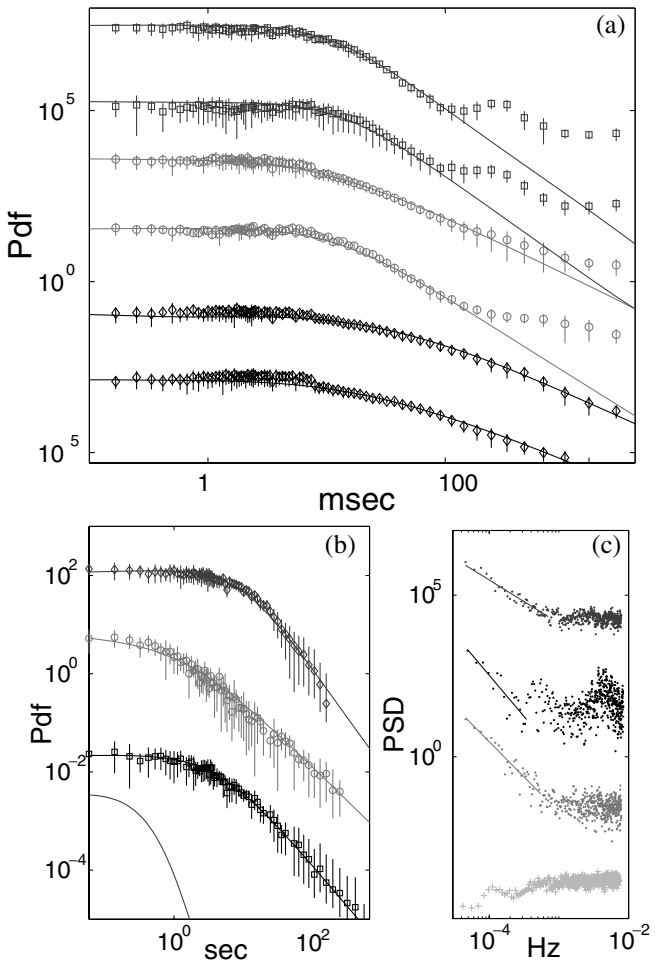

FIG. 3. Temporal statistics from the three network types: diamond: small, circle: medium, and square: large. Plots were vertically shifted for clarity. (a) Histograms of $\delta(i)$ for two neurons from each of the three network types. Fits to the data followed the maximum likelihood method of [14]. The range of fit parameters were $0.4 \leq \alpha \leq 1.4$ and $80 \leq \gamma \leq 1000$ for $n = 10$ neurons from each of the three network types. (b) Histograms of $\Delta(i)$ for each network type. Fit parameters: (1) small, $\alpha = 1.05 \pm 0.09$, $\gamma = 26 \pm 7.6$ ($n = 3$), (2) medium, $\alpha = 1.05 \pm 0.47$, $\gamma = 260 \pm 210$ ($n = 3$), and (3) large, $\alpha = 1.13 \pm 0.2$, $\gamma = 88 \pm 65$ ($n = 3$). For comparison, a Gaussian distribution obtained from simulations of the integrate and fire (I&F) model is plotted at the bottom (solid line). (c) Power spectrum estimation (periodogram) of the three network types and I&F model simulations: large (top), medium (second from top), small (second from bottom), and simulation (bottom).

(Fig. 3b). A statistical analysis of all networks yielded $\alpha = 1.05 \pm 0.09$, 1.07 ± 0.47, and 1.13 ± 0.2 for the small, medium, and large size networks, respectively. For comparison, a simulation of the leaky integrate and fire model with a dynamical threshold [15,16] was performed and produced a Gaussian IEI-increment distribution (see Fig. 3b).

Gerstein and Mandelbrot [17] proposed that the ISI distribution of the neurons themselves may obey a Lévy distribution (as distinct from the increments we have studied). Wise [18], who studied *in vivo* neural recordings, showed the existence of a bimodal ISI distribution consisting of a fast horizontal component followed by a long-tail decay. The above may be consistent with our observations of the increments' Lévy distribution.

The Lévy distribution provides insight about the scaling behavior in distribution. Characterization of the time series extending to longer time scales can be deduced from frequency-domain statistics such as autocorrelation and power spectral functions. In particularly long signals, containing large fluctuations and nonstationary trends, the power spectrum can be estimated by calculating the count-based periodogram [19]. The data set is divided into contiguous segments of equal length T. Within each segment, a discrete sequence $\{W_m\}$ is formed by further dividing T into M equal bins and then counting the number of events within each bin. A discrete Fourier transform $\tilde{W}(f)$ of length M is then calculated for each of the segments. Finally, $\tilde{W}(f)$ is averaged over segments to obtain $S(f)$—the periodogram of the sequence.

The SBE power-spectral estimators in all networks were found to obey a power-law decay $S(f) \sim f^{\eta}$ for low frequencies, regardless of network size (Fig. 3). The structure over low frequencies is indicative of long-range autocorrelations in the bursting activity, with positive correlations on time scales of minutes and hours, since $\eta < 0$. These correlations might indicate that the networks have the capability to sustain biological memory. Again for comparison, a simulation of the leaky integrate and fire method was performed and produced a nearly flat power spectral density.

Our observations show that networks of all sizes share two basic temporal features: scale invariance (Lévy distribution) on time scales of ISIs and IEIs and long-range correlations. The former often reflects a self-organizing feature of excitable systems which are composed of many nonlinearly coupled subsystems [9,10,20,21]. These features are present at both the single cell and network levels and are shared by networks of all sizes. Looking at the individual neurons, we find that ISI increments follow the Lévy statistics up to the 100-ms time scale, which corresponds to the width of the SBE. This implies a separation of time scales between the neuron activity and the network behavior. Thus, the Lévy distribution on the network level reflects the emergent properties of the network in which the neurons are the subsystems. With respect to the neurons, it implies that they are also composed of nonlinearly coupled subsystems—the ionic channels.

A comparison of the activity of isolated and self-contained biological networks with that of artificial neural networks may yield important insight on organizational principles of network dynamics. Current models, however, do not agree with our observations; rather, they exhibit Gaussian increment distributions and lack long-time autocorrelations. Thus, our observations suggest that new models must be developed [12].

In addition, artificial neural networks of different sizes typically exhibit very different levels of activity (e.g., mean density of SBE in time; see [22,23] for discussion). The similarity in the activities of different-size networks suggests that these networks are self-regulated to produce the observed scale-invariant and long-range correlated behavior and to sustain their mean level of activity. For example, such self-regulation could be achieved by an adjustment of synaptic efficacies or neuronal firing threshold [16].

It has been suggested [3] that large neuronal networks self-organize into functional subunits of the order of several millimeters in size. The above interpretation may agree with the temporal structures we observed in the small ~1-mm networks (see Fig. 2b) and in the spectral structures of the medium-size networks (see Fig. 3c). In a separate publication we will quantify and discuss the emergence of this temporal clustering effect.

We have greatly benefited from conversations with D. Horn, I. Golding, and B. Kol. We are thankful to I. Brainis for technical assistance. This research has been partially supported by a grant from the Israeli Academy of Sciences, the Sackler Institute, the Adams Super Center for Brain Studies, and the Kodesh Institute.

*Corresponding author.
Email address: eshel@venus.tau.ac.il

[1] M. Camepari, M. Bove, E. Maede, M. Cappello, and A. Kawana, Biol. Cyber. **77**, 153–162 (1997).

[2] E. R. Kandel, J. H. Schwartz, and T. M. Jessel, *Essentials of Neural Science and Behavior* (Appleton & Lange, Norwalk, CT, 1995).

[3] H. P. C. Robinson, M. Kawahara, Y. Jimbo, K. Torimitsu, Y. Kuroda, and A. Kawana, J. Neurophysiol. **70**, 1606–1616 (1993).

[4] Dissociated cultures of cortical neurons from one-day-old Charles River rats were prepared and maintained as described previously [16,24]. The cultures were maintained in growth conditions at 37 °C with 5% CO_2 and 95% humidity prior to and during measurements. Neuronal networks with defined geometries were grown as follows: Cells were plated at a density of 3×10^6 cells/dish (dish radius = 11 mm) on MEAs patterned with a poly-d-lysine (PDL) substrate. Ten minutes after plating, dishes were rinsed with growth medium to remove unattached cells. The protocol for PDL patterns fabrication is as follows: The surface was spin coated to obtain a ~2-μm-thick photoresist (PR, 5214e, Hoechst) layer, which was exposed and developed through a patterned mask. After development, the patterns are transferred to the PR layer. The surface was then rinsed in water and immersed overnight in a 100-μg/ml PDL water solution. After drying in air, the surface is left with a thick PDL coating. The wafer is immersed for 2–3 s in an ultrasonic acetone bath, which removes the PR, leaving PDL patterns in the PR-free areas. Continuous, noninvasive extracellular recordings from an array of 60 substrate-integrated thin film microelectrodes (MEA chip, Multi-Channel Systems, Germany [7]). The signal was transferred to a computer via an array of amplifiers (Multi-Channel Systems) and read using Alpha Map data acquisition software (Alpha Omega Engineering, Israel). In a typical experiment, neuronal action potentials were successfully recorded from approximately half of the recording electrodes. Off-line analysis and spike sorting of the extracellular recordings were performed by our wavelet packets decomposition method [24], yielding 1–3 neuronal signals per electrode. In this way, time sequences of (up to 300 000) action potentials were obtained from single neurons.

[5] Y. Jimbo, H. P. C. Robinson, and A. Kawana, IEEE Trans. Biomed. Eng. **40**, 804–810 (1993).

[6] B. C. Wheeler and G. J. Brewer, in *Enabling Technologies for Cultured Neuronal Networks* (Ref. [8]), p. 167.

[7] U. Egert, B. Schlosshauer, S. Fennrich, W. Nisch, M. Fejtl, T. Knott, T. Muller, and H. Hammerle, Brain. Res. Protoc. **2**, 229–242 (1998).

[8] G. W. Gross, in *Enabling Technologies for Cultured Neural Networks,* edited by David A. Stenger and Thomas M. McKenna (Academic Press, San Diego, CA, 1994), pp. 277–313.

[9] C. K. Peng, J. Mietus, J. M. Hausdorff, S. Havlin, H. E. Stanley, and A. L. Goldberger, Phys. Rev. Lett. **70**, 1343 (1993).

[10] R. N. Mantegna and H. Eugene Stanley, Nature (London) **376**, 46–49 (1995).

[11] M. F. Shlesinger, G. M. Zaslavsky, and J. Klafter, Nature (London) **363**, 31 (1993).

[12] Y. Soen and E. Braun, Phys. Rev. E **61**, R2216 (2000).

[13] N. Cohen, H. G. Rotstein, and E. Braun (to be published).

[14] J. P. Nolan, report.

[15] C. Koch, *Biophysics of Computation* (Oxford University Press, New York, 1999).

[16] R. Segev, Y. Shapira, M. Benveniste, and E. Ben-Jacob, Phys. Rev. E **64**, 011920 (2001).

[17] G. L. Gerstein and B. Mandelbrot, Biophys. J. **4**, 41–68 (1964).

[18] M. E. Wise, Stat. Distribution Sci. Work **6**, 211 (1981).

[19] S. B. Lowen, T. Ozaki, E. Kaplan, B. E. A. Saleh, and M. C. Teich, Methods **24**, 377–394 (2001).

[20] R. N. Mantegna and H. Eugene Stanley, Nature (London) **383**, 587–588 (1996).

[21] E. Ben-Jacob, I. Cohen, and H. Levine, Adv. Phys. **49**, 395–554 (2000).

[22] L. F. Abbott and Sacha B. Nelson, Nat. Neurosci. **3**, 1178–1183 (2000).

[23] G. G. Turrigiano, K. R. Leslie, N. S. Desai, L. C. Rutherford, and S. B. Nelson, Nature (London) **391**, 892–896 (1998).

[24] E. Hulata, R. Segev, Y. Shapira, M. Benveniste, and E. Ben-Jacob, Phys. Rev. Lett. **85**, 4637 (2000).